Estimating the dimension of a fractal point process

Steven B. Lowen and Malvin C. Teich

Columbia University, Department of Electrical Engineering
New York, NY 10027

ABSTRACT

We discuss issues involved in estimating the dimension of a fractal point process. We first define the term fractal point process and provide some examples of experimental phenomena for which they serve as suitable models. We then develop mathematical formulations of fractal point processes, and present two methods for dimension estimation and an analysis of their performance. Finally, we compare this analysis with results from both simulated and natural examples of fractal point processes.

1. DEFINITION OF A FRACTAL POINT PROCESS

Some phenomena occur at discrete times (or places), with the individual events largely identical. Examples include the detection of particles from radioactive decay and the times of sunrise at a particular location. A point process is a mathematical construction which represents these events as points in a space, and is either stochastic, when associated with random phenomena like radioactive decay, or deterministic, as in the case of sunrises. For a stochastic point process, the statistics of this set of points provide information about the underlying structure of the phenomenon under study. A *fractal* stochastic point process results when these statistics exhibit power-law scaling, indicating that the represented phenomena contains clusters of points over all (or a relatively large set of) time or length scales [1, 2, 3, 4]. Fractal deterministic point processes exist as mathematical entities, such as those generating strange attractors, and when applied to physical phenomena are closely related to chaos theory. Since an extensive body of literature already exists in this area, we do not consider deterministic processes further in this paper. The dimension of a fractal point process is a measure of the clustering of the points within the process; it lies between a lower limit of zero (the dimension of a point), and an upper limit equal to the dimension of the space in which the process is embedded [1]. In this paper we consider point processes on a line, so that the upper limit is unity.

2. APPLICATIONS OF FRACTAL POINT PROCESSES

Many phenomena in the physical world may be readily represented by fractal point processes. A few are listed below.

2.1. Auditory-nerve-fiber action potentials

Nerve fibers transmit information by means of action potentials, which are localized regions of depolarization traveling down the length of an axon. Action potentials on a given axon are brief and largely identical events, so their detection at a recording electrode may be well represented by a point process. Fractal point processes describe the action potentials in auditory-nerve fibers [2, 5, 6]. Although over short time scales nonfractal point processes prove superior for representing such nerve spikes, over long time scales (typically greater than one second) fractal behavior becomes evident. In particular, both the Fano factor and the power spectral density, two measures discused later in this paper) are found to vary in a power-law fashion over these long time scales, and estimators of the rate of the process converge more slowly than would be expected for nonfractal processes, displaying fluctuations which are self-affine over varying time scales greater than one second.

2.2. Openings of ion channels

Ion channels are openings in the membranes of cells which permit ions to diffuse in or out [7]. These channels are usually specific to a particular ion, or group of related ions, and block the passage of other species of ions. Further, most

 0-8194-1285-6/93/$6.00

channels have gates, and thus the channels may be either open or closed. In most cases intermediate conduction states are not observed. A few ion channels may be modeled by a two-state Markov process, with one state representing the open channel, and the other representing the closed channel. This model generates exponentially distributed dwell times in both states. However, many ion channels exhibit power-law distributed closed times between open times of negligible duration [8], and are well described by a fractal point process. Indeed, count moments of all orders, coincidence rates, and power spectral densities all vary as power laws, indicating fractal behavior.

2.3. Trapping times in amorphous semiconductors

The multiple trapping model, as developed by Orenstein and Kastner [9, 10] and Tiedje and Rose [11], shows how exponentially distributed traps over a large range of energies lead to a power-law decay of current in an amorphous semiconductor. If a pulse of light strikes such a semiconductor, the many carriers excited out of their traps will be available to carry current until they are recaptured by a trap, which happens relatively quickly. At some point each carrier will be released from its trap by thermal excitation and become mobile for a time, and then be recaptured by another trap. For exponentially distributed states with identical capture cross sections, the electrons tend to be trapped in shallow states at first, but the probability of being caught in a deep trap increases as time progresses. This leads to a current that decreases as a power-law function of time.

The multiple trapping model may be usefully recast in terms of fractal point processes [4, 12]. Consider an amorphous semiconductor with localized states (traps) that are exponentially distributed with parameter E_0 between a minimum energy E_L of the order of $\kappa\mathcal{T}$, where κ is Boltzmann's constant and $\mathcal{T}$ is the absolute temperature; and a maximum energy E_H determined by the bandgap. For a particular trap with energy $\mathcal{E}$, the corresponding mean waiting time is

$$\tau = \tau_0 \exp(\mathcal{E}/\kappa\mathcal{T}), \tag{1}$$

where τ_0 is the average vibrational period of the atoms in the semiconductor. If we define characteristic time cutoffs $A \equiv \tau_0 \exp(E_L/\kappa\mathcal{T})$ and $B \equiv \tau_0 \exp(E_H/\kappa\mathcal{T})$, and the power-law exponent $D \equiv \kappa\mathcal{T}/E_0$, then the mean waiting time τ has a density which decays as a power law between those two cutoffs. Each trap holds carriers for times that are exponentially distributed given the conditional parameter τ, and averaging this exponential density over all possible values of τ yields the unconditional trapping time density, which is itself approximately power law:

$$p(t) \approx D\Gamma(D+1)A^D t^{-(D+1)}, \tag{2}$$

for $A \ll t \ll B$. Thus each carrier will be trapped for a period that is essentially power-law distributed.

Upon escaping from a trap, the carrier can conduct current for a short time until it is again captured by another trap. Thus each carrier executes a series of current-carrying jumps well described by a fractal point process. Assuming that each carrier acts independently of the others, the action of the carriers as a whole can be modeled as the superposition of several component fractal point processes, which is another fractal point process. Again, both experimental [13] and theoretical [14] results point to a power-law or fractal decay in the power spectral density, while other statistics also show scaling behavior.

2.4. Electronic burst noise

Burst noise occurs in many communications systems and is characterized by relatively brief noise events which cluster together, separated by relatively longer periods of quiet. Mandelbrot [15] long ago showed that burst errors in communication systems are well modeled by a version of a fractal renewal process, and in particular that the interevent times were essentially independent of each other for time scales determined by the resolution and the duration of the observation.

3. MATHEMATICAL FORMULATIONS OF FRACTAL POINT PROCESSES

We have defined three fractal point processes and derived a number of their statistics:

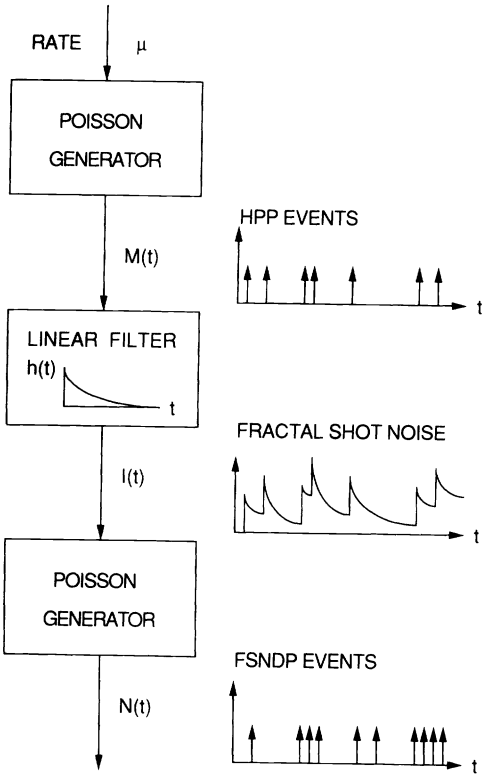

Figure 1: A primary homogeneous Poisson point process $M(t)$ with constant rate μ serves as the input to a linear filter with impulse response function $h(t)$. The continuous-time stochastic process $I(t)$ at the output of this filter is shot noise, which serves as the random rate for another Poisson point process, whose output is $N(t)$. $N(t)$ is a special doubly stochastic Poisson point process (DSPP), known as a shot-noise driven Poisson point process (SNDP). If $h(t)$ decays in power-law fashion, then $I(t)$ is fractal shot noise and $N(t)$ is a FSNDP.

3.1. Fractal renewal process

Perhaps the simplest fractal point process is the fractal renewal process (FRP) [4, 12, 15]. For the FRP, the times between adjacent events are independent random variables T drawn from the same fractal probability distribution. In particular, the survivor function $1 - P(t)$ decays as a power law

$$1 - P(t) = \Pr\{T > t\} = \begin{cases} k/t^D & \text{for } A < t < B, \\ 0 & \text{otherwise.} \end{cases} \tag{3}$$

The FRP exhibits fractal behavior over time scales between A and B. Another point process results from the superposition of a number of independent FRPs, for which fractal behavior is observed over a smaller range of time scales. The effective cutoff at short times increases with the number of superposed FRPs.

3.2. Fractal-shot-noise-driven Poisson process

The fractal-shot-noise-driven Poisson process (FSNDP) consists of two Poisson processes separated by a linear filter with a power-law decaying impulse response function [3] (see Fig. 1).

The one-dimensional homogeneous Poisson point process (HPP) is perhaps the simplest stochastic point process [16]. The HPP is characterized by a single constant quantity, its rate, which is the number of events expected to occur in a

unit interval. A fundamental property of the HPP is that it is memoryless; knowledge of the entire history and future of a given realization of a HPP yields no information about the behavior of the process at the present.

Other point processes do not share this memoryless property, and therefore cannot be described in terms of a constant rate. An important example of an inhomogeneous point process is the doubly stochastic Poisson point process (DSPP) [17]. For this point process, the rate itself varies stochastically. Thus the DSPP displays two forms of randomness: that associated with the stochastically varying rate, and that associated with the underlying Poisson nature of the process even if its rate were constant.

The FSNDP is a special case of the DSPP. Here the rate of the Poisson process is determined by fractal shot noise, which is itself a filtered version of another homogeneous Poisson point process. Figure 1 schematically illustrates the FSNDP as a two-stage stochastic process. The first stage is a HPP with constant rate μ. Its output $M(t)$ becomes the input to a linear filter with a power-law decaying impulse response function $h(t)$, which then produces fractal shot noise $I(t)$ at its output. This fractal shot-noise process becomes the time varying rate for the last stage, a second Poisson point process. The resulting point process $N(T)$ is not homogeneous, but rather exhibits the variations of the fractal shot noise driving process. Thus the two forms of randomness inherent in the DSPP are, in the FSNDP, two separate Poisson processes, linked by a power-law varying linear filter.

3.3. Fractal-Gaussian-noise-driven Poisson process

Under suitable conditions, the underlying fractal shot noise of the FSNDP converges to a Gaussian probability density, as provided by the central limit theorem, and therefore becomes fractal Gaussian noise [18]. The resulting point process becomes a fractal-Gaussian-noise-driven Poisson process (FGNDP) [3]. The superposition of many independent FRPs, mentioned above, also converges to a FGNDP for certain ranges of parameters [4].

The FGNDP is important because Gaussian processes are ubiquitous, well understood, and may be completely described by their means and autocovariance functions; thus comparison with experiment becomes easy. Indeed, the FGNDP provides an excellent model for the sequence of action potentials in primary auditory-nerve fibers, requiring only three parameters [2, 6]. With the inclusion of the refractory effects of nerve fibers, the FGNDP describes the behavior of nerve spikes in auditory fibers in several mammalian species over all time scales and for a broad variety of statistical measures.

3.3. Other fractal point processes

Other important formulations of fractal point processes exist. Grüneis and colleagues defined such a process where each member in a sequence of primary events gives rise to a train of secondary events (as in the FSNDP), but where the events in a train form a segment of a renewal process, with a fractal (power-law distributed) duration [19]. The resulting process indeed exhibits power-law scaling in the same statistics as the FSNDP [20].

4. FRACTAL DIMENSION ESTIMATION: THEORY

Fractal processes by their nature display fluctuations over a broad range of time scales, including long ones, so that estimating the properties of a segment of data presents more difficulties than estimating those of a nonfractal process. For example, the estimate of the mean of a fractal process has a variance which decreases only slowly with the length of the data segment [2, 6]. For a nonfractal point process, such as the HPP, the variance decreases as T^{-1}, where T is the length of the segment; for a fractal point process, such as the FGNDP, the variance decreases more slowly, as T^{D-1} where D is the fractal dimension of the point process [21]. This slow convergence derives from the fractal nature of the process, implying long-range correlations which do not average out nearly as quickly as independent fluctuations. As a result of these long-range variations, detecting a change in a property of a fractal process generally requires a prohibitively large quantity of data, and in fact is not a practical goal in many cases.

In this paper we take as a given that the data segment under study derives from a stationary process. Consequently,

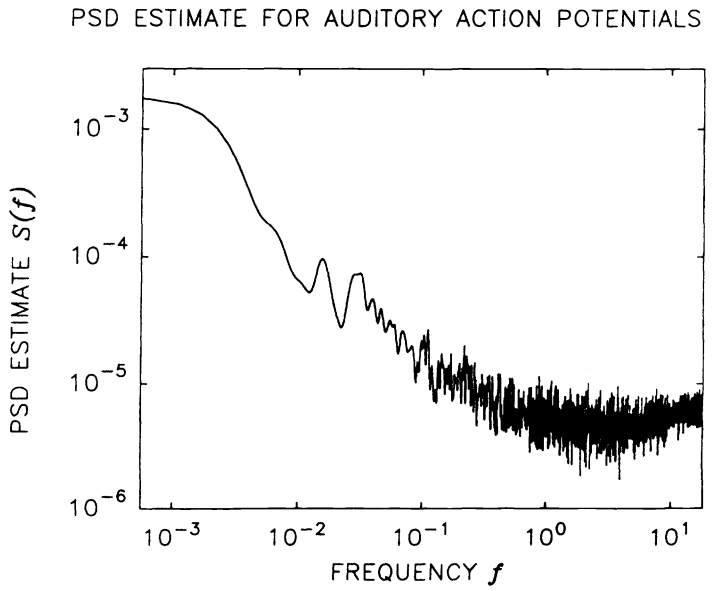

Figure 2: Doubly logarithmic plot of power spectral density estimate of the point process recorded from an auditory-nerve fiber under continuous-tone stimulation (without modulation). The data segment has a duration of 1800 s, with an average time between events of 14.11 ms. The estimate was smoothed with a triangular window in the time domain (autocorrelation) of length equal to 1/8 the duration of the data segment. Over long time scales (low frequencies) the shape of the curve follows a straight line of slope −0.717 indicating fractal behavior.

while a process may exhibit large fluctuations which imply a large fractal dimension, any data segment obtained from it has a non-zero probability of lacking these fluctuations and therefore appearing to be from a process with a smaller fractal dimension [22]. This phenomena provides an appreciable bias for shorter data segments, and often a surprisingly long set of data is required before reliable estimates of the fractal dimension may be obtained.

Given a segment of a fractal point process, we wish to estimate the fractal dimension, D. Many statistical measures may be applied to a point process, but some, such as the interevent histogram, provide information over short time scales [23], and are therefore not useful in determining the character of long-term fluctuations. Two statistics which provide useful information about the fractal dimension are the power spectral density (PSD) and the Fano-factor time curve (FFC).

4.1. Power spectral density

The PSD provides a measure of how the power in a process is concentrated in various frequency bands [24]. For a fractal process, the PSD decreases as an inverse power-law function of frequency, with the exponent equal to the fractal dimension. Often the PSD of a fractal point process will approach an asymptotic value at high frequencies, and assumes the form

$$S(f) = S_0 \left[1 + (f/f_0)^{-D}\right], \tag{4}$$

where f_0 represents the white-noise cutoff frequency. A PSD of a representative recording of auditory-nerve action potentials is provided in Fig. 2.

To estimate the fractal dimension D, we begin by partitioning the data segment into N adjacent windows of equal length, and counting the number of points that fall in each window, resulting in a sequence of counts $\{z_n\}_{n=0}^{N-1}$. We chose N large enough so that the PSD estimate has negligable bias, and small enough so that the counting windows are large compared to the average time between points; then by the central limit theorem the number of counts in each window approximates a Gaussian distribution. We then compute the discrete Fourier transform of this sequence, yielding the (unsmoothed) estimate of the power spectral density $\mathcal{S}(k)$. Each of the values of $\mathcal{S}(k)$ provides information independent

of the other values (for large N), and has a error which is also independent of the other errors [25]. A typical estimate will have the form

$$\mathcal{S}(k) = S_0[1 + (k/k_0)^{-D}]e^{n(k)} \tag{5}$$

for $k > 0$, where D is the dimension of the fractal point process, and k_0 represents this white-noise cutoff frequency in the integer-frequency space indexed by k. To obtain the best estimate of D, we further require that the number of windows N be chosen to be greater than k_0. The random variable $n(k)$ represents the error in the kth value in the power spectral density estimate, and does not depend on $\mathcal{S}(k)$ [25]. We then have

$$\begin{aligned} \mathrm{E}\{e^{n(k)}\} &= 1 \\ \mathrm{E}\left\{\left[e^{n(j)} - 1\right]\left[e^{n(k)} - 1\right]\right\} &= \delta_{jk}. \end{aligned} \tag{6}$$

To obtain the variance of n_k we need the distribution of n_k. However, the result depends only weakly on this distribution, so in the interests of tractability we make the assumption that the distribution is Gaussian, yielding

$$\begin{aligned} \overline{n} \equiv \mathrm{E}\{n(k)\} &= -\ln(2)/2 \\ \mathrm{E}\{[n(j) - \overline{n}][n(k) - \overline{n}]\} &= \ln(2)\delta_{jk}. \end{aligned} \tag{7}$$

To estimate D, we perform a least-squares fit on the logarithm of the power spectral density estimate (less the asymptotic value for high frequencies $\mathcal{S}_0$) versus the logarithm of the index k, using the first k_0 values. For $k \geq k_0$ there is essentially no additional information, so we ignore these values. Since each value in $\mathcal{S}(k)$ for $1 \leq k < k_0$ provides essentially the same amount of information, and all are independent, there is no reason to weight any one of them more than the others in estimating D. Define $x_k \equiv \ln(k)$, and $y_k \equiv \ln[\mathcal{S}(k) - \mathcal{S}_0] = \ln(S_0) + D\ln(k_0) - D\ln(k) + n(k)$. Then the estimate of D is simply the covariance of $\{x\}$ and $\{y\}$ divided by the variance of $\{x\}$

$$\begin{aligned} \mathcal{D} &= -\frac{(k_0 - 1)^{-1}}{(k_0 - 1)^{-1}} \times \frac{\displaystyle\sum_{k=1}^{k_0} x_k y_k - k_0^{-1}\left(\sum_{k=1}^{k_0} x_k\right)\left(\sum_{j=1}^{k_0} y_j\right)}{\displaystyle\sum_{k=1}^{k_0} x_k^2 - k_0^{-1}\left(\sum_{k=1}^{k_0} x_k\right)^2} \\ &= D + \frac{k_0^{-2}\displaystyle\sum_{k=1}^{k_0}[n(k) - \overline{n}]\sum_{j=1}^{k_0}\ln(j) - k_0^{-1}\sum_{k=1}^{k_0}[n(k) - \overline{n}]\ln(k)}{f(k_0)}, \end{aligned} \tag{8}$$

where

$$f(j) \equiv \frac{1}{j}\sum_{k=1}^{j}\ln^2(k) - \left[\frac{1}{j}\sum_{k=1}^{j}\ln(k)\right]^2 \tag{9}$$

is the variance of $\ln(j)$. The function $f(j)$ rises monotonically to an asymptotic value of unity as $j \to \infty$.

The second term in Eq. (8) contains sums of zero-mean random variables, so that $\mathrm{E}\{\mathcal{D}\} = D$, and $\mathcal{D}$ is an unbiased estimate. The variance of $\mathcal{D}$ is given by

$$\begin{aligned} \mathrm{Var}[\mathcal{D}] &= \mathrm{E}\left\{\left[\frac{1}{k_0^2}\sum_{k=1}^{k_0}[n(k) - \overline{n}]\sum_{j=1}^{k_0}\ln(j) - \frac{1}{k_0}\sum_{k=1}^{k_0}[n(k) - \overline{n}]\ln(k)\right]^2\right\}\frac{1}{f^2(k_0)} \\ &= \frac{\ln(2)}{k_0 f(k_0)}. \end{aligned} \tag{10}$$

As the length T of the data segment increases, the effective white-noise cutoff frequency k_0 will increase proportionately, and the variance of the estimate $\mathcal{D}$ will decrease as T^{-1}, in contrast to the variance of the estimate of the mean.

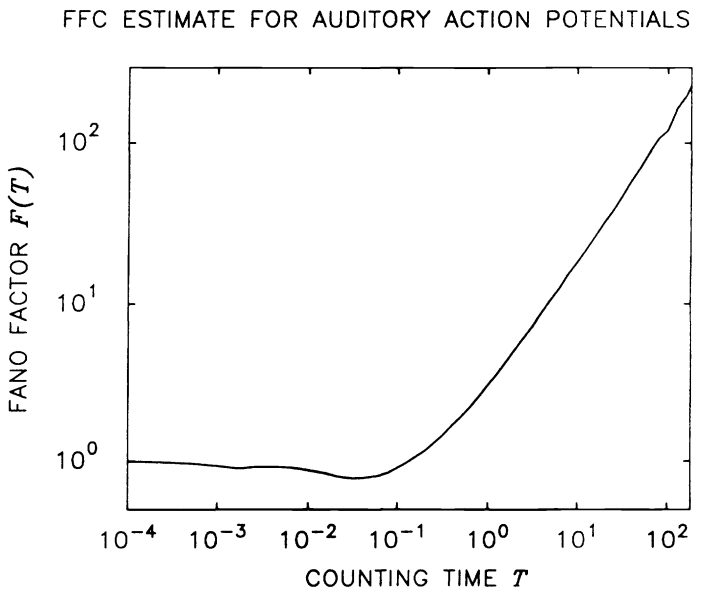

Figure 3: Fano-factor time curve estimate of the same point process as in Fig. 2. Over long time scales the shape of the curve follows a straight line of slope 0.840 indicating fractal behavior with essentially the same dimension as in Fig. 2.

4.2. Fano-factor time curve

Another statistic that is particularly useful over long time scales is the Fano factor $F(T)$, defined as the variance of the number of counts in a specified time window T divided by the mean number of counts. For the HPP, the Fano factor assumes a value of unity for any counting time. For other point processes, the Fano factor varies with the counting time, and the form of $F(T)$ as a function of T, called the Fano-factor time curve (FFC), provides useful information about the point process under study. In particular, for a fractal point process, the FFC (ignoring refractory effects) has the functional form

$$F(T) = 1 + (T/T_0)^D, \tag{11}$$

where D is again the dimension of the fractal point process, and T_0 is an intercept time. Thus another estimate of D may be obtained by performing linear regression on $\ln[F(T) - 1]$ versus $\ln(T)$, as in Eq. (8). A FFC constructed from the same recording of auditory-nerve action potentials as in Fig. 2 is provided in Fig. 3.

The properties of this estimate are considerably more difficult to derive. Since the estimate of the mean will have the same proportional error for all counting times T, this will have no effect on the estimate of D and can be ignored. However, the estimation of the variance, particularly at long counting times, will suffer from the same slow convergence problems as the determination of the mean. Heuristically, estimates of the power-law slope are restricted to counting times less than one tenth of the length of the data segment.

The FFC-based estimate of D also differs from that of the PSD in having a maximum possible value of unity, while the PSD may have any slope. This may be seen by considering a data segment divided into $2N$ intervals of length T, with z_j representing the number of events falling within the jth interval. The data segment may also be divided into N intervals of length $2T$, with Z_i events in the ith interval. Then estimates of the mean values of z and Z are related simply by $\langle Z \rangle = 2\langle z \rangle$ by construction, and for the mean square

$$\begin{aligned} \langle Z^2 \rangle &= N^{-1} \sum_{i=0}^{N-1} Z_i^2 = N^{-1} \sum_{i=0}^{N-1} (z_{2i} + z_{2i+1})^2 \\ &= N^{-1} \sum_{i=0}^{N-1} (2z_{2i}^2 + 2z_{2i+1}^2 - z_{2i}^2 - z_{2i+1}^2 + 2z_{2i} z_{2i+1}) \end{aligned}$$

$$= 2N^{-1}\sum_{j=0}^{2N-1} z_j^2 - N^{-1}\sum_{j=0}^{N-1}(z_{2j} - z_{2j+1})^2$$

$$\leq 2N^{-1}\sum_{j=0}^{2N-1} z_j^2 = 4\langle z^2\rangle. \tag{12}$$

For the estimates of the variances $\mathcal{V}$ of z and Z, and assuming a large value of N, then

$$\mathcal{V}_Z = \langle Z^2\rangle - \langle Z\rangle^2 \leq 4\langle z^2\rangle - (2\langle z\rangle)^2 = 4\mathcal{V}_z, \tag{13}$$

and for the estimates of the Fano factor

$$F(2T) = \frac{\mathcal{V}_Z}{\langle Z\rangle} \leq \frac{4\mathcal{V}_z}{2\langle z\rangle} = 2F(T). \tag{14}$$

Therefore, the estimate of D obtained from the FFC must be less than unity. This maximum value of the FFC-based estimate effectively skews the estimate towards lower values for D close to unity. The skew and the slow convergence of the variance estimate yield qualitative information about the statistics of the FFC-based estimate, but for more quantitative information we must rely on numerical simulations.

The FFC and the PSD are uniquely determined by each other through the coincidence rate $G(\tau)$, defined as

$$G(\tau) \equiv \lim_{\Delta\to 0} \frac{\Pr\{\mathcal{E}(t, t+\Delta) \text{ and } \mathcal{E}(t+\tau, t+\tau+\Delta)\}}{\Delta^2}, \tag{15}$$

where $\mathcal{E}(x, y)$ represents the occurrence of at least one event of the point process in the interval (x, y) [26]. The coincidence rate and PSD are Fourier transforms of each other, and the FFC may be obtained from the coincidence rate by an integral transform

$$F(T) = 1 + \frac{2}{\lambda T}\int_0^T (T-\tau)\left[G(\tau) - \lambda^2\right] d\tau, \tag{16}$$

where λ is the average rate of events of the point process. These relationships verify that the fractal dimensions obtained from the PSD and the FFC are indeed the same number [2], and provide a relationship between the intercept time T_0 and the white-noise cutoff frequency f_0

$$2\pi T_0 f_0 = \left[\Gamma(D+2)\cos(D\pi/2)\right]^{1/D}. \tag{17}$$

Since the two estimators of D employ information over roughly the same time scales, and derive from the same underlying value, we expect their statistics to be similar.

5. FRACTAL DIMENSION ESTIMATION: SIMULATIONS AND EXPERIMENTS

5.1. Simulation: dead-time-modified (DTM) FSNDP

To facilitate comparison with experimental auditory-nerve data, and to provide results indicative of practical data analysis, we chose statistics for the DTM-FSNDP simulation from typical primary auditory nerve-fiber spike trains. The average time between action potentials was taken to be 15 ms, the fractal intercept time was set at $T_0 = 100$ ms, the duration of each simulation was $T_{max} = 100$ s, and refractoriness was approximated by a fixed dead time of $T_d = 2$ ms. One hundred simulations were performed for each of three values of the fractal dimension: $D = 0.2$, 0.5, and 0.8.

Estimates of the fractal dimension were obtained by least-squares fit of doubly-logarithmic versions of the FFC. For counting times shorter than 2 s the Fano factor exhibited excessive negative bias due to the effects of dead time; counting times were limited to a maximum of 10 s due to variance of the Fano factor. Figure 4 presents histograms of the estimated dimension for the three values of the simulated dimension, while Table 1 presents aggregate statistics. As

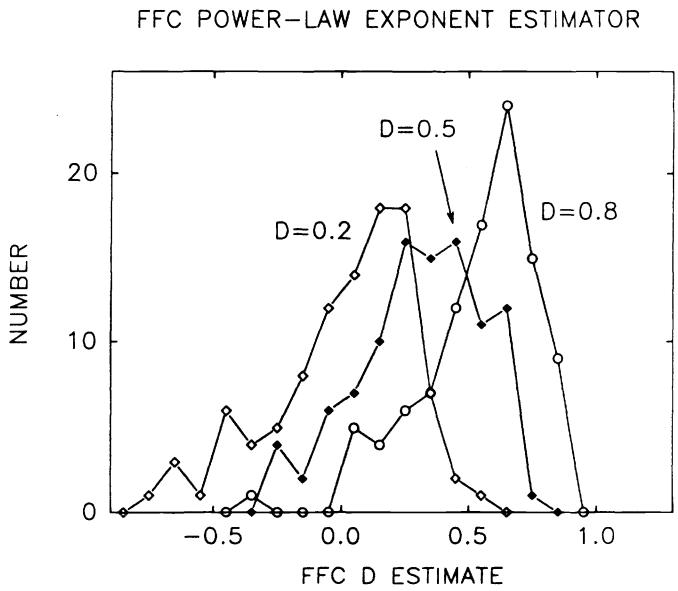

Figure 4: Histograms of estimates of the fractal dimension obtained by least-squares fits of doubly-logarithmic versions of Fano-factor time curve estimates computed between counting times of 2 s and 10 s. These estimates were obtained from simulations of the FSNDP with an average time between points of 15 ms, a fractal intercept time $T_0 = 100$ ms, a duration $T_{max} = 100$ s, and a fixed dead time of $T_d = 2$ ms. One hundred simulations were performed for each of three values of the fractal dimension: $D = 0.2$ (hollow diamonds), 0.5 (filled diamonds), and 0.8 (hollow cirlces). All curves exhibit a negative bias and a spread about the mean. No values in excess of unity were observed.

Table 1: Statistics of fractal-dimension estimators for 100 trials.

		DTM-FSNDP Simulation			Auditory
		$D = .2$	$D = .5$	$D = .8$	experiment
FFC:	Average	.012	.313	.539	.504
	Standard Deviation	.275	.245	.224	.213
PSD:	Average	.043	.318	.636	.574
	Standard Deviation	.175	.194	.237	.222
Correlation Coefficient		.693	.622	.757	.784

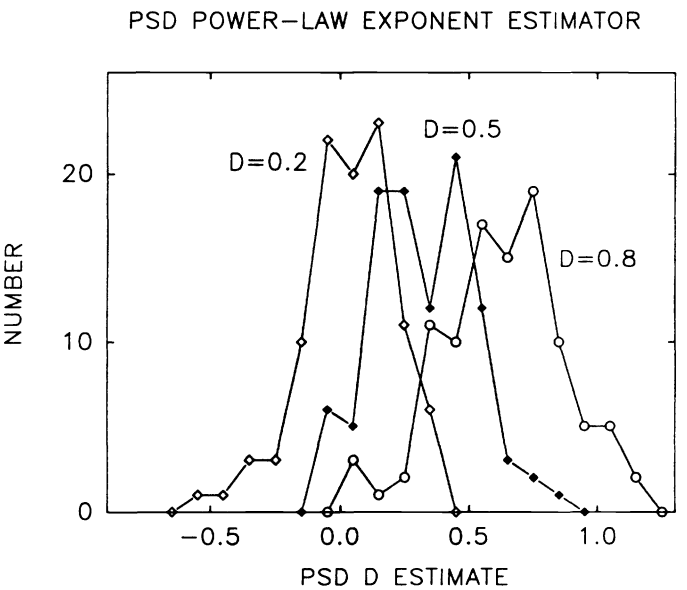

Figure 5: Histograms of estimates of the fractal dimension obtained by least-squares fits of doubly-logarithmic versions of power spectral density estimates computed between frequencies of 0.25 Hz and 0.01 Hz. These estimates were obtained from the same simulations of the FSNDP as in Fig. 4, and use the same symbols. All curves exhibit a negative bias and a spread about the mean.

expected, the FFC-based estimates of the fractal dimension show a bias towards smaller values, indicating that for many of the simulations long-term fluctuations did not occur or were underrepresented. In addition, the estimates display a significant spread about the mean, also due to the fractal fluctuations. The maximum value of the FFC slope provides the expected absolute cutoff of unity, and none of the three hundred simulations displayed an estimated slope greater than this limit.

Performing a least-squares fit on doubly-logarithmic versions of the PSD provided complementary estimates of the fractal dimension. Here, reliable time scales extend to the length of the data segment, but are limited at short times by both dead-time effects and by the white-noise cutoff frequency; a range of 0.25 Hz to 0.01 Hz appears to give the best performance. Figure 5 presents histograms of the estimated dimension for the three values of the simulated dimension, while Table 1 again presents aggregate statistics. As with the FFC, the PSD provides estimates of the fractal dimension with a similar bias toward smaller values. Since the two statistics agree, it is unlikely that both estimators yield inaccurate information about the data segments under consideration; rather fractal sporadicity in the fluctuations provides the best explanation. Any finite-length data segment of a fractal point process may lack these fluctuations and therefore appear to be from a process with a smaller fractal dimension [22]. The standard deviation of the PSD-based fractal dimension may be easily computed from Eq. (10) to be $\sigma_{\mathcal{D}} = 0.204$, in excellent agreement with values obtained from the simulations, which have an aggregate average of 0.202. In contrast to the FFC, there is no absolute cutoff at unity.

Joint statistics of the FFC- and PSD-based estimators describe how information is shared between these two statistics. Figure 6 presents scatterplots of the values obtained from the two estimators for all three hundred simulations, and Table 1 contains values of the correlation coefficient. Both show a significant correlation between the two estimators, expected since they estimate the same underlying dimension D. This provides still more reason to favor fractal sporadicity in the fluctuations as an explanation for the bias seen in both estimators.

5.2. Experiment: auditory-nerve action potentials

A similar analysis was performed on the long (1800-s) segment of data recorded from an auditory nerve fiber under

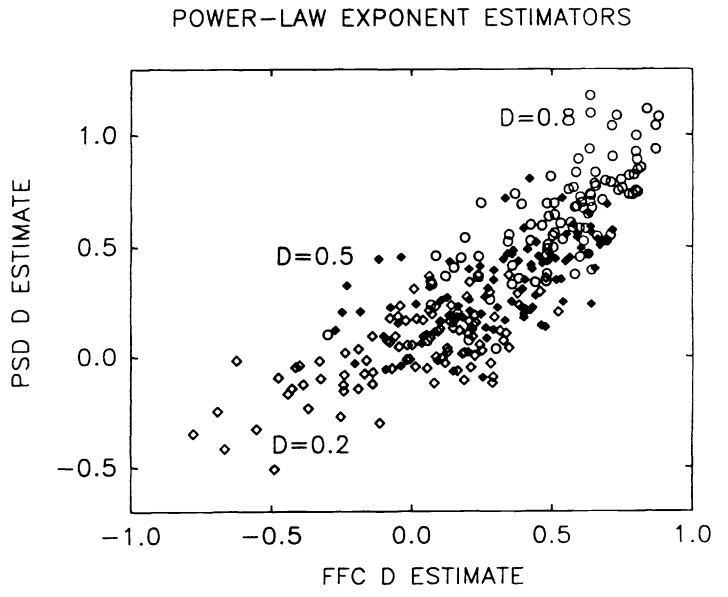

Figure 6: Scatterplot comparing estimates of the fractal dimension from Fano-factor-time-curve and power-spectral-density estimates. Estimates of the fractal dimension computed from the Fano-factor time curve as in Fig. 4 form the abcissa, while the ordinate consists of estimates from the power spectral density. Symbols are as in Fig. 4. Correlation between the two estimates is apparent.

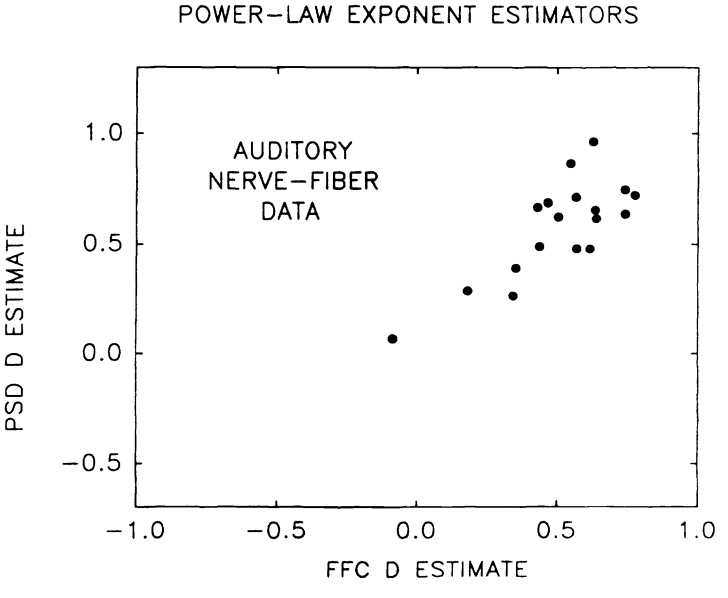

Figure 7: Scatterplot comparing estimates of the fractal dimension from Fano-factor-time-curve and power-spectral-density estimates, obtained from the auditory-nerve data used in Figs. 2 and 3. Again, correlation between the two estimates is apparent.

continuous-tone stimulation (see Figs. 2 and 3). The data were divided into segments of 100 s each, with the resulting statistics displayed in the last column of Table 1. A scatterplot is provided in Fig. 7. The standard deviation of the PSD-based estimate of the fractal dimension, like those computed from the simulations, agrees well with the theoretical value of 0.204. Results for the auditory-nerve data resemble those for the simulations, with an underlying fractal dimension of nearly 0.8. Indeed, lines fit to the FFC and PSD computed over the entire 1800-s duration of the data (displayed in Figs. 2 and 3) yields estimated fractal dimensions of 0.840 and 0.717 respectively, in good agreement with this figure. Thus the FSNDP again proves to be an excellent simulation for primary auditory nerve-fiber data.

6. CONCLUSION

We have addressed some of the issues surrounding estimating the dimension of a fractal point process. We have defined fractal point processes, and provided examples of mathematical formulations for them. We have discussed the nature of fractal fluctuations and how they affect estimation of fractal dimension in general, and for two useful estimators in particular. Finally, we provided results from simulations and experimental data to support our approach.

7. ACKNOWLEDGMENTS

This work was supported by the Joint Services Electronics Program throught the Columbia Radiation Laboratory by the Office of Naval Research under Grant No. N00014-92-J-1251, and by the National Science Foundation through the Center for Telecommunications Research at Columbia University.

8. REFERENCES

[1] B. B. Mandelbrot, *The Fractal Geometry of Nature*. Freeman, New York, 1983.

[2] M. C. Teich, "Fractal neuronal firing patterns," in *Single Neuron Computation*, edited by T. McKenna, J. Davis, and S. Zornetzer, pp. 589-625, Academic, Boston, 1992.

[3] S. B. Lowen and M. C. Teich, "Doubly stochastic Poisson point process driven by fractal shot noise," *Phys. Rev. A* **43**, pp. 4192-4215, 1991.

[4] S. B. Lowen and M. C. Teich, "Fractal renewal processes generate $1/f$ noise," *Phys. Rev. E* **47**, pp. 992-1001, 1993.

[5] M. C. Teich, "Fractal character of the auditory neural spike train," *IEEE Trans. Biomed. Eng.* **36**, pp. 150-160, 1989.

[6] M. C. Teich, R. G. Turcott, S. B. Lowen, "The fractal doubly stochastic Poisson point process as a model for the cochlear neural spike train," in *The Mechanics and Biophysics of Hearing (Lecture Notes in Biomathematics, Vol. 87)*, edited by P. Dallos, C. D. Geisler, J. W. Matthews, M. A. Ruggero, and C. R. Steele, pp. 354-361, Springer-Verlag, New York, 1990.

[7] B. Sakmann and E. Neher, *Single-Channel Recording*. Plenum, New York, 1983.

[8] L. S. Liebovitch and T. I. Tóth, "Using fractals to understand the opening and closing of ion channels," *Ann. Biomed. Eng.* **18**, pp. 177, 1990.

[9] J. Orenstein, M. A. Kastner, and V. Vaninov, "Transient photoconductivity and photo-induced optical absorption in amorphous semiconductors," *Phil. Mag. B*, **46**, pp. 23-62, 1982.

[10] M. A. Kastner, "The peculiar motion of electrons in amorphous semiconductors," in *Physical Properties of Amorphous Materials*, edited by D. Alser, B. B. Schwartz, and M. C. Steele, pp. 381-396, Plenum, New York, 1985.

[11] T. Tiedje and A. Rose, "A physical interpretation of dispersive transport in disordered semiconductors," *Solid State Commun.* **37**, pp. 49-52, 1980.

[12] S. B. Lowen and M. C. Teich, "Fractal renewal processes as a model of charge transport in amorphous semiconductors," *Phys. Rev. B* **46**, pp. 1816-1819, 1992.

[13] V. K. Bhatnagar and K. L. Bhatia, "Frequency dependent electrical transport in bismuth-modified amorphous germanium sulfide semiconductors," *J. Non-cryst. Sol.* **119**, pp. 214-231, 1990.

[14] W. Tomaszewicz, "Multiple-trapping carrier transport due to modulated photogeneration," *Phil. Mag. Lett.* **61**, pp. 237-243, 1990.

[15] B. B. Mandelbrot, "Self-similar error clusters in communication systems and the concept of conditional stationarity," *IEEE Trans. Comm. Tech.* **13**, pp. 71-90, 1965.

[16] F. A. Haight, *Handbook of the Poisson Distribution*, Wiley, New York, 1967.

[17] D. R. Cox, "Some statistical methods connected with series of events," *J. Roy. Stat. Soc.* **B 17**, pp. 129-164, 1955.

[18] S. B. Lowen and M. C. Teich, "Power-law shot noise," *IEEE Trans. Info. Theory* **36**, pp. 1302-1318, 1990.

[19] F. Grüneis and H.-J. Baiter, "More detailed explication of a number fluctuation model generating $1/f$ pattern," *Physica* **136A**, pp. 432-452, 1986.

[20] F. Grüneis and T. Musha, "Clustering Poisson process and $1/f$ noise," *Jpn. J. Appl. Phys.* **25**, 1504-1509, 1986.

[21] M. C. Teich, D. H. Johnson, A. R. Kumar, and R. G. Turcott, "Rate fluctuations and fractional power-law noise recorded from cells in the lower auditory pathway of the cat," *Hear. Res.* **46**, pp. 41-52, 1990.

[22] M. Meesman, F. Grüneis, P. Flachenecker, and K. Kniffki, "A new method for analysis of heart rate variability: counting statistics of $1/f$ fluctuations," *Biol. Cybern.* **68**, pp. 299-306, 1993.

[23] S. B. Lowen and M. C. Teich, "Auditory-nerve action potentials from a nonrenewal point process over short as well as long time scales," *J. Acoust. Soc. Am.* **92**, pp. 803-806, 1992.

[24] A. Papoulis, *Probability, Random Variables, and Stochastic Processes*, 3rd Edition, McGraw-Hill, New York, 1991.

[25] A. V. Oppenheim and R. W. Schafer, *Digital Signal Processing*, Prentice-Hall, Englewood Cliffs, New Jersey, 1975.

[26] D. R. Cox and P. A. W. Lewis, *The Statistical Analysis of Series of Events*, Methuen, London, 1966.